Supporting Information for

Cu_7S_4 Nanosheets Enriched with Cu–S Bond for Highly Active and Selective CO_2 Electroreduction to Formate

Yan Wen[a], Nan Fang[a], Wenqiang Liu[a], Tang Yang[a], Yong Xu, [b,*] and Xiaoqing Huang[a,*]

[a] State Key Laboratory of Physical Chemistry of Solid Surfaces, College of Chemistry and Chemical Engineering, Xiamen University, Xiamen, 361005, China. E-mail: hxq006@xmu.edu.cn.

[b] Guangzhou Key Laboratory of Low-Dimensional Materials and Energy Storage Devices, Collaborative Innovation Center of Advanced Energy Materials, School of Materials and Energy, Guangdong University of Technology, Guangzhou, 510006, China. E-mail: yongxu@gdut.edu.cn

1. Experimental Section

1.1 Chemicals.

Copper thiocyanate (CuSCN, 99.0%), copper (II) chloride dihydrate ($CuCl_2 \cdot 2H_2O$, 99.0%), hexadecyl trimethyl ammonium bromide (CTAB, $C_{19}H_{42}BrN$, 99.0%) and potassium hydroxide (KOH, 85.0%) were purchased from Shanghai Macklin Biochemical Co. Ltd. Catechol ($C_6H_6O_2$, 99.0%) and oleylamine ($C_{18}H_{37}N$, 80–90%) were purchased from Aladdin Industrial Corp. Oleic acid ($C_{18}H_{34}O_2$, 85.0%) was purchased from Tokyo Chemical Industry. All the chemicals were used as received without further purification. The water (18 MΩ cm^{-1}) used in all experiments was prepared by passing through an ultra-pure purification system (Aqua Solutions)

1.2 Synthesis of Cu_7S_4 nanosheets (NSs).

Briefly, CuSCN (38.4 mg) and pyrocatechol (60 mg), oleylamine (4 mL) and oleic acid (1 mL) were added into a vial (volume: 30 mL). After the vial had been capped, the mixture was ultrasonicated for 30 min. The resulting homogeneous mixture was heated from room temperature to 180 °C in 30 min and maintained at 180 °C for 2 h in an oil bath before cooling room temperature. The products were collected by centrifugation and washed three times with a cyclohexane/ethanol mixture.

1.3 Synthesis of CuO nanosheets (NSs).

Briefly, $CuCl_2 \cdot 2H_2O$ (500mg), CTAB (500mg) and H_2O (20ml) were added into a vial (volume: 30 mL). After the vial had been capped, the mixture was ultrasonicated for 30 min to form a blue solution. Then, 1 mL NaOH aqueous solution (0.3 g/ml) was dropwise added into the above-mentioned solution. After ultrasonication for 30 min, the resulting homogeneous mixture was heated from room temperature to 120 °C in 30 min and maintained at the same temperature for 6 h in an oil bath before cooling to room temperature. The products were collected by centrifugation and washed three times with ethanol and distilled water, and then dried under vacuum at 60 °C for 12 h.

1.4 Preparation of Cu_7S_4/C, Cu_7S_4/C-250 and Cu_7S_4/C-350.

Cu_7S_4 NSs were deposited on Vulcan XC72R carbon with ultrasonication for 30 min in 10 mL cyclohexane. The products were washed three times with cyclohexane/ethanol. The obtained Cu_7S_4/C was dried at 60 °C in an oven for 12 h and then annealed at 250 °C in Ar for 1 h. Afterwards, Cu_7S_4/C was annealed at 250 °C and 350 °C in air for 1 h, respectively, to obtain Cu_7S_4/C-250 and Cu_7S_4/C-350.

1.5 Material Characterization.

The high-angle annular dark-field scanning trans-mission electron microscopy (HAADF-STEM), HAADF-STEM energy-dispersive X-ray spectroscopy (HAADF-STEM-EDS), and high-resolution TEM (HRTEM) were operated on FEI Tecnai F30 TEM (USA) at an accelerating voltage of 300 kV. Powder X-ray diffraction (XRD) patterns were recorded on a Rigaku Ultima IV diffractometer using Cu Kα radiation (40 kV, 30 mA). Low-magnification TEM was conducted on a JEM-1400 electron microscope at an accelerating voltage of 100 kV. Scanning electron microscopy (SEM) measurements were performed on a Hitachi S-4800 operated at 20 kV. X-ray photoelectron spectroscopy (XPS) was conducted on SSI S-Probe XPS spectrometer. The carbon peak at 284.6 eV was used as a reference to correct for charging effects AT-FTIR.

1.6 Electrode preparation.

The cathode gas diffusion electrode (GDE) were prepared by spraying the catalyst inks on the microporous hydrophobic side of gas diffusion carbon paper (GOOSS UNION 22BB). The catalyst ink of Cu_7S_4 NSs was prepared by dispersing 1 mL nanocrystalline in cyclohexane in the presence of 20 μL Nafion (DuPont D520, 5 wt%) through ultrasonication. The final mass loading of the catalyst is maintained to be ~0.22 mg cm^{-2}. The catalysts inks of Cu_7S_4/C,Cu_7S_4/C-250 and Cu_7S_4/C-350 were prepared by dispersing the 1mL nanocrystalline in ethanol in the presence of 20 μL Nafion through ultrasonication. The final mass loading of the catalyst is maintained to be ~1.5 mg cm^{-2}.

1.7 Electrochemical measurements and Product Analysis.

All electrochemical measurements were performed in a flow cell composed of a GDE, an anion exchange membrane and a platinum sheet anode as shown in Figure S4. The electrolysis was controlled by a CHI 660e electrochemical workstation equipped with a high current amplifier CHI 680c. Saturated Ag/AgCl was used as the reference and it was calibrated with respect to RHE: $E_{(RHE)} = E_{(Ag/AgCl)} + 0.197 + pH \times 0.0592$. All of the electrocatalytic reactions were conducted at ambient pressure and temperature. Potassium hydroxide was typically used as the electrolyte and was circulated through the electrochemical cell using a peristaltic pump. High-purity CO_2 was supplied to the cathode with a constant flow rate monitored by a mass flow controller. Unless otherwise stated, the reaction was conducted in 1 M KOH with a flow rate of 30 ml min^{-1} for 30 min and the gas flow rate was 30 ml min^{-1}. During the electrolytic reaction, the effluent gas from the cathode compartment went through the sampling loop of a gas chromatograph and was analysed on line. H_2 was analysed with a thermal conductivity detector. CO, methane and ethylene were analysed with a flame ionization detector. The liquid products (formate, acetate, ethanol and n-propanol) were analysed by ^{1}H NMR spectroscopy. The ^{1}H NMR spectrum was recorded on an Advance III 500-MHz Unity plus spectrometer (Bruker), in which 0.5 ml of the electrolyte was mixed with 0.1 ml DMSO (internal standard, diluted to 1000 ppm (v/v) by deuterated water). The gaseous products were sampled and analysed on line every 15 min during the reaction, and the averaged result was used for discussion. The liquid products were collected and analysed after the operation for 20 min. There is no IR compensation during all tests.

1.8 Electrochemical in situ Attenuated Total Reflection Flourier Transformed Infrared Spectroscopy (ATR-FTIR).

Electrochemical in situ Attenuated Total Reflection Flourier Transformed Infrared Spectroscopy (ATR-FTIR) was employed to trace the signals of the intermediates using a Nicolet Nexus 670 Spectroscopy equipped with a liquid nitrogen-cooled mercury-cadmium-telluride (MCT) detector. An ECIR-II cell equipped with a Pike Veemax III ATR in a three-electrode system was provided from Shanghai Linglu Instrument& Equipment Co. To improve the signal intensity, the monocrystal silicon was initially coated with a layer of Au using the chemical plating method. Then, 20 μL catalyst ink (similar to section 1.5) was dropped on the surface of the Au film and served as the working electrode. Platinum sheet and Ag/AgCl electrode were used as counter electrodes and reference electrodes, respectively. Before the test, the CO_2 feeding gas was purged into the electrolyte for 30 minutes and continuously bubbled during the measurement. The potential-dependent in situ ATR-FTIR tests were carried out with LSV test from 0 V to –1.0 V (vs. RHE) with a scan rate of 5 mV s^{-1}.

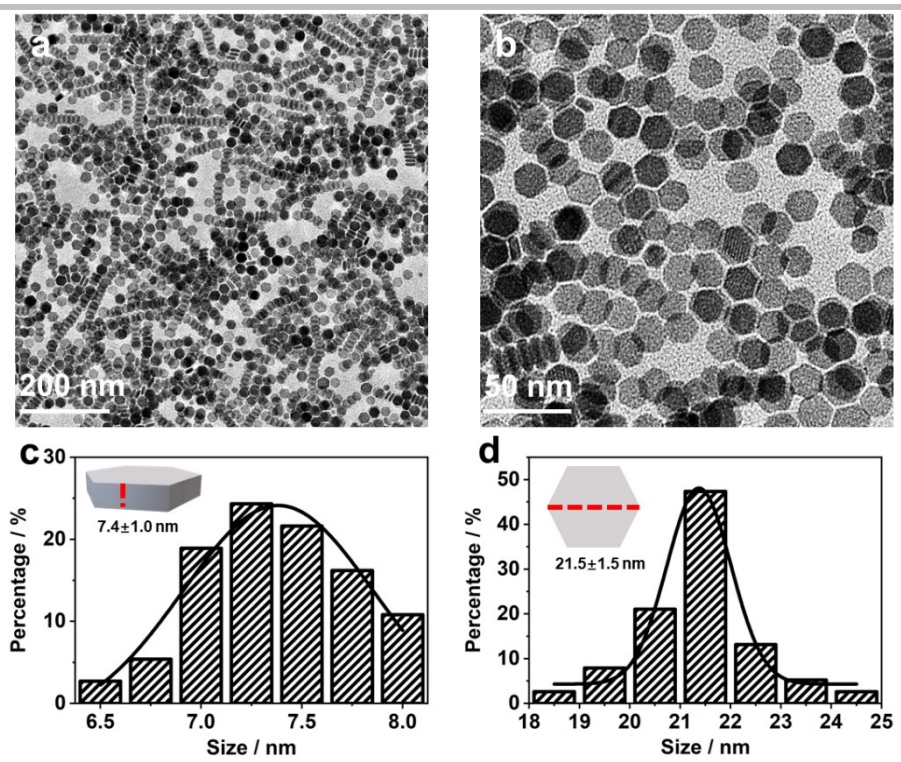

Figure S1. (a, b) TEM images, (c) thickness, and (d) lateral size of Cu_7S_4 NSs.

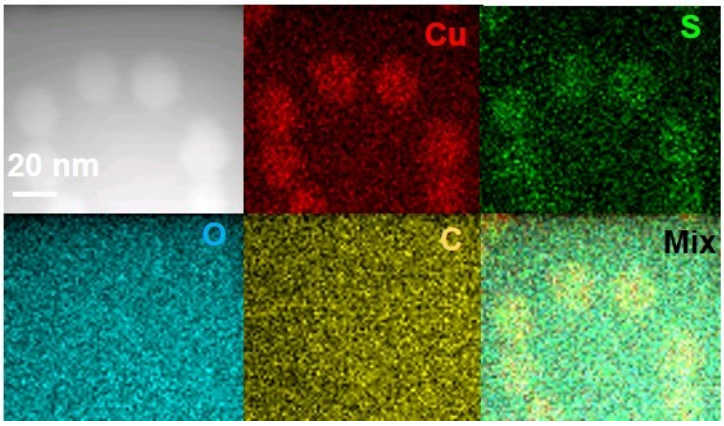

Figure S2. HAADF-STEM image with elemental mappings of Cu_7S_4 NSs (include O and C).

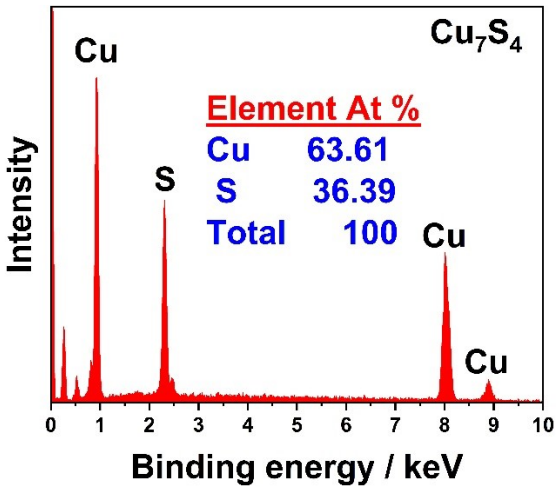

Figure S3. SEM-EDS spectrum of Cu_7S_4 NSs.

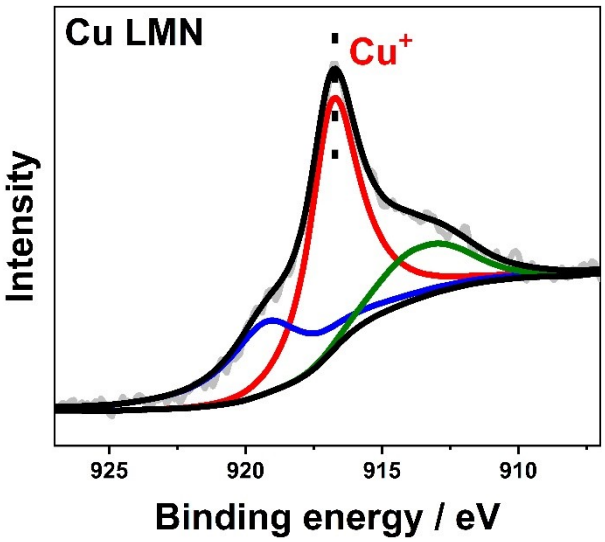

Figure S4. Cu LMN Auger spectra of Cu_7S_4 NSs.

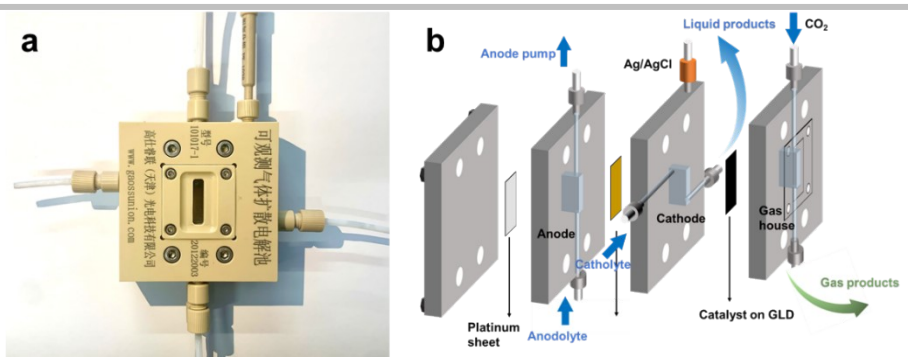

Figure S5. The photographand scheme of the observable gas diffusion electrode.

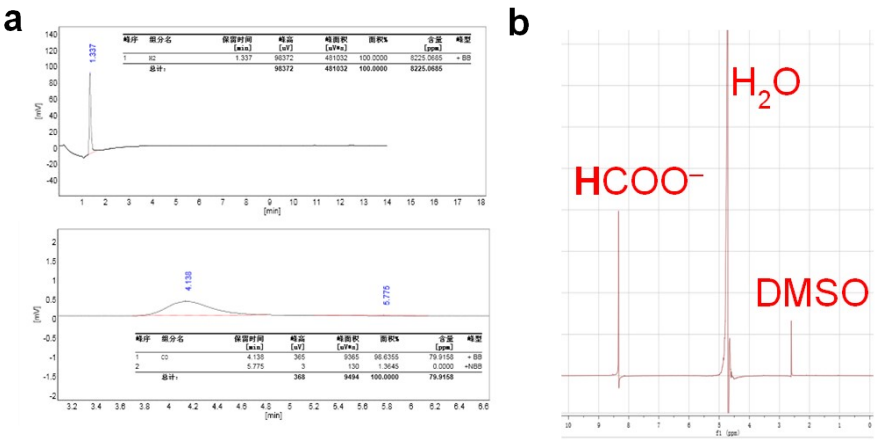

Figure S6. (a) H_2 and CO_2 peaks in gas chromatography (GC) profiles collected at –200 mA cm^{-2} on Cu_7S_4 NSs. (b) ^1H nuclear magnetic resonance (^1H-NMR) spectrum of the electrolyte after CO_2RR over Cu_7S_4 NSs at –200 mA cm^{-2}.

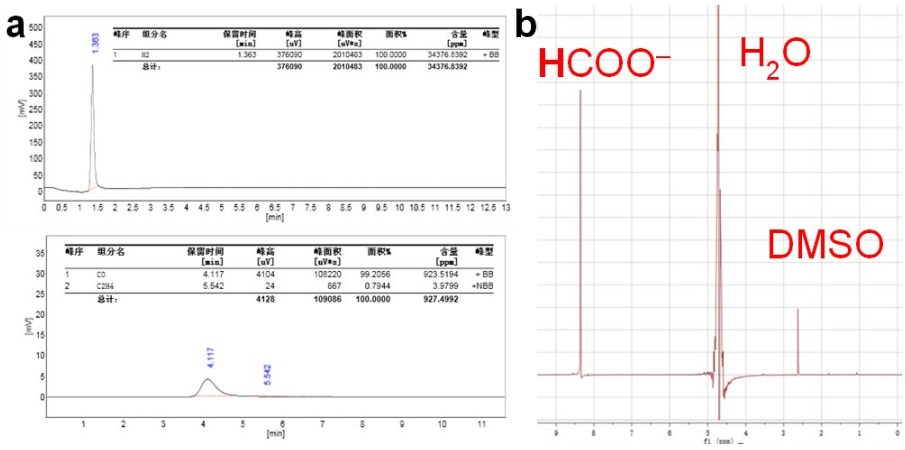

Figure S7. (a) H_2 and CO_2 peaks in gas chromatography (GC) profiles collected at –600 mA cm^{-2} on Cu_7S_4 NSs. (b) ^1H nuclear magnetic resonance (^1H-NMR) spectrum of the electrolyte after CO_2RR over Cu_7S_4 NSs at –600 mA cm^{-2}.

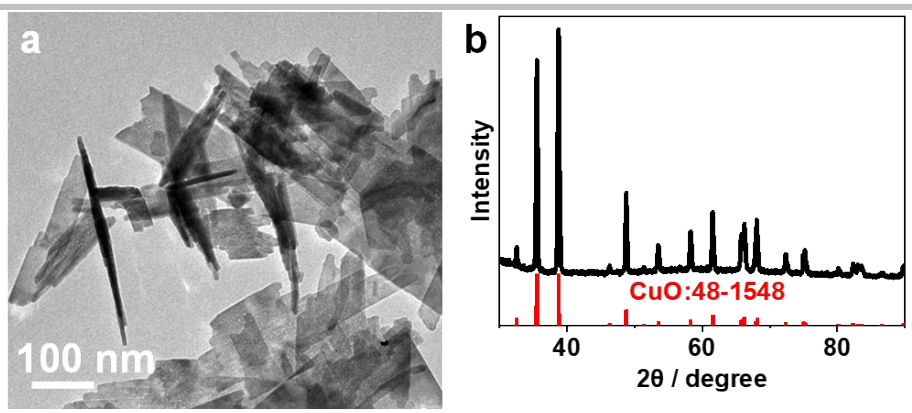

Figure S8. (a) TEM image and (b) XRD pattern of CuO NSs.

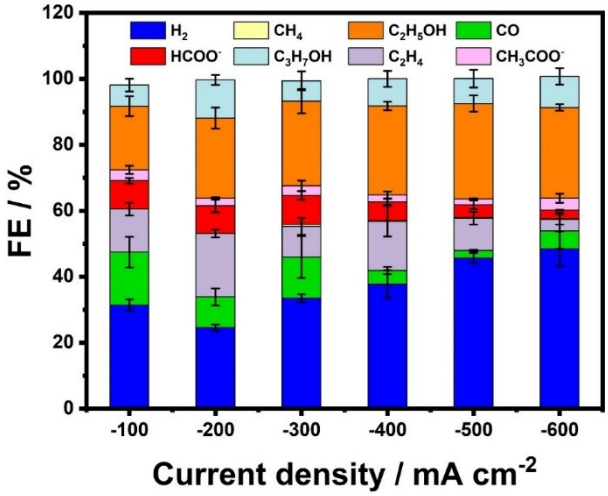

Figure S9. FEs of products during CO_2RR over CuO NSs at different current densities.

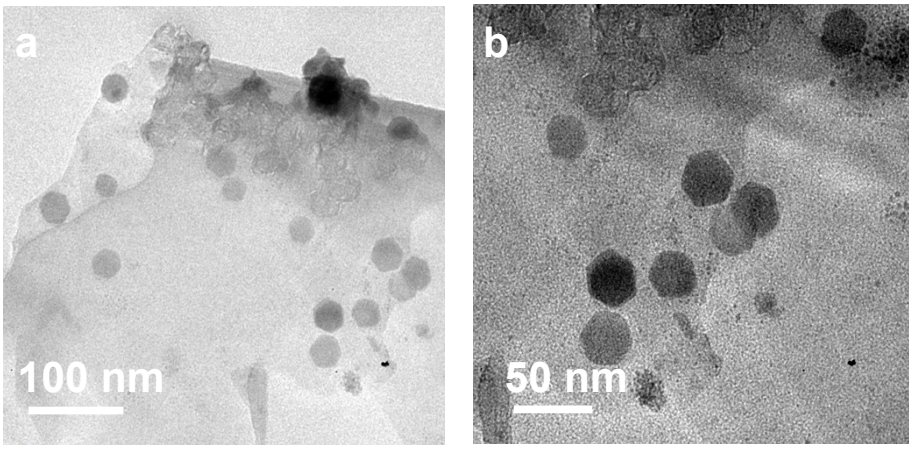

Figure S10. (a, b) TEM images of Cu_7S_4 NSs after CO_2RR at –200mA cm^{-2} for 5 h.

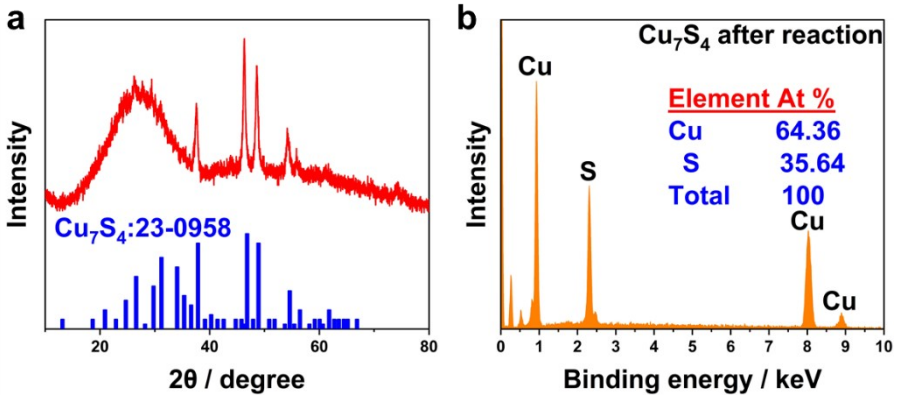

Figure S11. (a) XRD pattern and (b) SEM-EDS profile of Cu_7S_4 NSs after CO_2RR at –200mA cm^{-2} for 5 h.

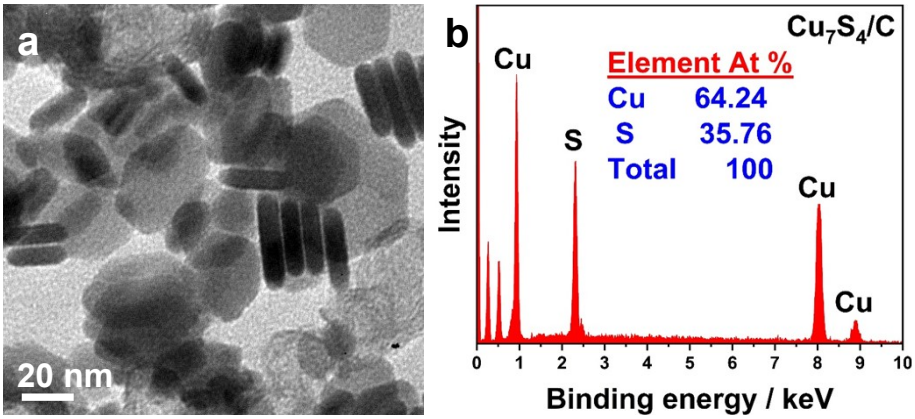

Figure S12. (a) TEM image and (b) SEM-EDS profile of Cu_7S_4/C.

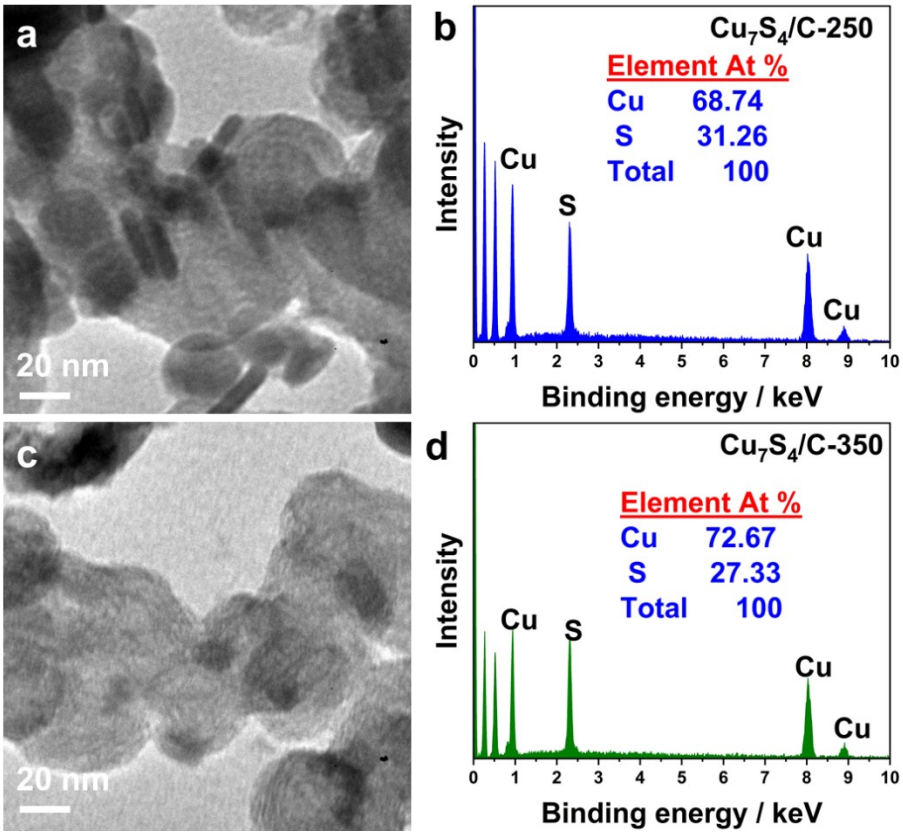

Figure S13. (a) TEM image and (b) SEM-EDS profile of Cu_7S_4/C-250. (c) TEM image and (d) SEM-EDS profile of Cu_7S_4/C-350.

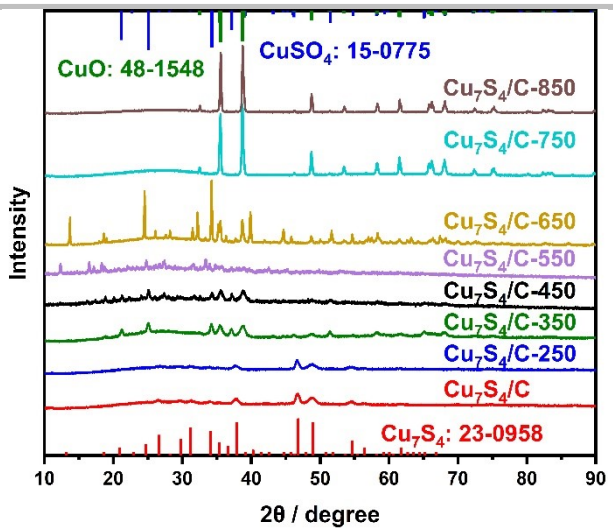

Figure S14. XRD pattern of Cu_7S_4/C after treat at different temperatures in air for 1 h.

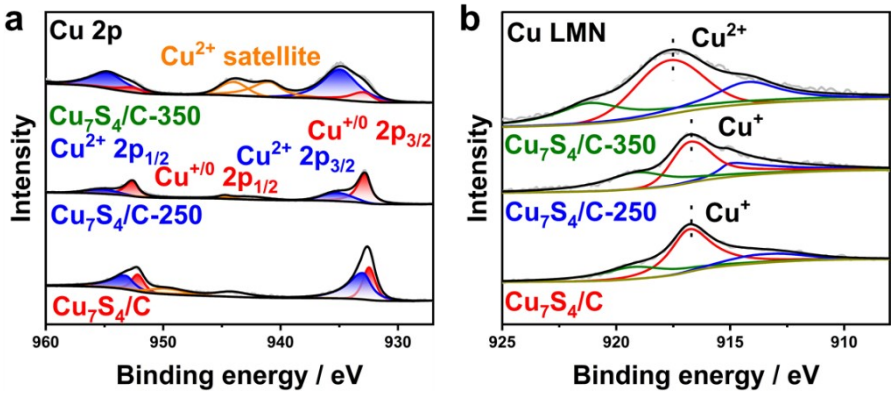

Figure S15. (a) Cu 2p XPS spectra and (b) Cu LMN Auger spectra of Cu_7S_4/C, Cu_7S_4/C-250 and Cu_7S_4/C-350.

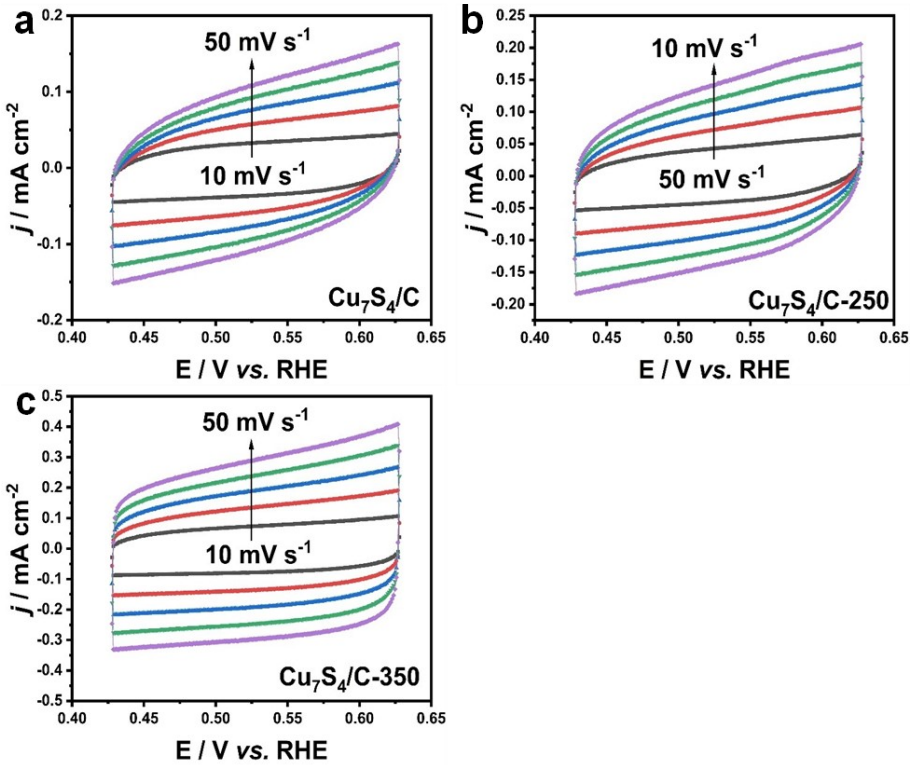

Figure S16. Electrochemically active surface areas (ECSA) measurements of (a) Cu_7S_4/C, (b)Cu_7S_4/C-250 and (c)Cu_7S_4/C-350. The potential window of cyclic voltammetric stripping was –0.4 V to –0.6 V versus Ag/AgCl (1 M KOH solution). The scan rates were 10, 20, 30, 40 and 50 mV s^{-1}, respectively.

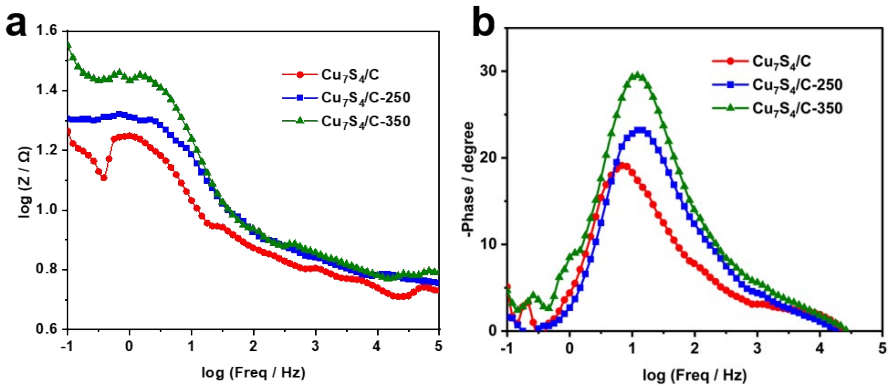

Figure S17. Bode plots of Cu_7S_4/C, Cu_7S_4/C-250 and Cu_7S_4/C-350.

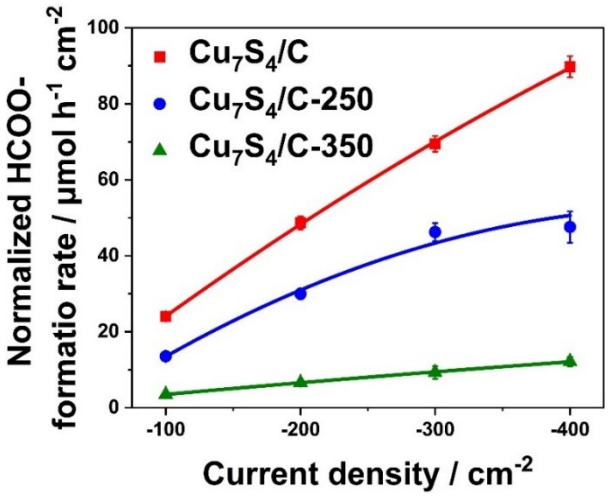

Figure S18. Normalized $HCOO^-$ formation rates by ECSA of Cu_7S_4/C, Cu_7S_4/C-250 and Cu_7S_4/C-350 under different applied potentials in 1.0 M KOH.

Table S1. Faradaic efficiency of products for CO_2RR over Cu_7S_4 NSs at different applied current densities.

Applied current density / mA cm^{-2}	FE H_2 / %	FE CO / %	FE $HCOO^-$ / %	FE Total / %
-100	18.4±1.0	0.4±0.1	79.6±1.2	98.3±0.2
-200	16.3±1.1	0.9±0.8	82.7±0.4	99.9±0.4
-300	16.8±0.6	0.9±0.5	82.0±1.3	99.7±1.5
-400	17.1±1.8	1.1±0.6	80.4±1.0	98.6±1.2
-500	20.7±0.5	1.8±.3	76.0±0.3	98.6±1.1
-600	22.8±0.2	1.1±0.9	76.0±3.0	99.9±2.7

Table S2. Comparison between the Cu_7S_4 NSs with other reported catalysts for CO_2RR to fromate.

Cell type	Catalyst	Electrolyte	$FE_{formate}$ / %	$J_{foamate}$ / mA cm^{-2}	Ref.
Flow cell	**Cu_7S_4**	**1 M KOH**	**82.7**	**165.5**	**This work**
Flow cell	**Cu_7S_4**	**1 M KOH**	**76.0**	**456.0**	**This work**
H cell	InS	0.5 M $KHCO_3$	93.0	84.0	1
Flow cell	ZnInS	1 M $KHCO_3$	99.3	298.0	2
H cell	Sn(S)/Au	0.1 M $KHCO_3$	93.2	55.0	3
H cell	Cu-2.0C on Cu foil	0.1 M $NaHCO_3$	87.0	19.1	4
H cell	S-modified Cu nanoparticles on GDL	0.1 M $NaHCO_3$	80.0	12.0	5
H cell	CuS_x	0.1 M $KHCO_3$	75.0	6.8	6
H cell	Sulfur-doped Cu on Cu disks	0.1 M $KHCO_3$	<60	13.9	7
H cell	hydrogen-incorporated SnS_2	0.1 M $KHCO_3$	87.0	24.4	8
H cell	Cu-CTAB	0.1 M $KHCO_3$	82.3	2.5	9
Flow cell	$CuPb_1$	0.5 M $KHCO_3$	96.0	800.0	10
Flow cell	Hierarchical Cu-S nanoflakes on GDL	1 M KOH	89.9	404.1	11
Flow cell	S-CuSn	0.5 M $KHCO_3$	96.4	241.0	12
Flow cell	$SnO_2/Cu_6Sn_5/CuO$	1 M KOH	95.6	67.0	13
Flow cell	Cu/Bi_2S_3	1 M KOH	97.5	285.0	14
Flow cell	Cu-SnO_2	1 M KOH	81.0	405.0	15

Table S3. Faradaic efficiency of products for CO_2RR over CuO NSs at different applied current densities.

Applied current density / mA cm^{-2}	FE H_2 / %	FE CO / %	FE C_2H_4 / %	FE CH_4 / %	FE $HCOO^-$ / %	FE CH_3COO^- / %	FE C_2H_5OH / %	FE C_3H_7OH / %	FE Total / %
-100	31.4±1.7	16.1±4.7	13.1±1.9	-	8.6±0.8	3.3±.2	19.3±3.0	6.4±1.9	98.1±0.3
-200	24.6±0.9	9.3±2.6	19.2±.2	-	8.4±2.0	2.2±.6	24.4±3.2	11.6±1.5	99.7±4.2
-300	33.5±1.2	12.5±6.3	9.3±2.6	0.6±0.5	8.8±1.3	2.9±1.6	25.7±3.7	6.2±2.9	99.4±2.1
-400	37.8±4.2	4.1±1.1	15.0±4.7	0.1±0.2	5.8±.9	2.1±1.1	27.0±1.3	8.3±2.4	100.0±1.2
-500	45.7±1.5	2.2±.3	9.8±1.9	0.2±0.0	3.9±1.3	1.8±0.2	28.9±2.5	7.6±2.7	100.1±0.8
-600	48.5±5.3	5.4±5.4	3.5±1.6	0.2±0.1	2.6±.2	3.6±1.4	27.5±1.0	9.5±2.5	100.8±1.6

Table S4. Faradaic efficiency of products for CO_2RR over Cu_7S_4/C at different applied current densities.

Applied current density / mA cm^{-2}	FE H_2 / %	FE CO / %	FE $HCOO^-$ / %	FE Total / %
-100	20.1±1.4	0.2±0.1	79.5±1.3	99.8±0.4
-200	19.2±2.8	0.17±0.1	80.4±2.9	99.8±0.1
-300	22.2±2.2	0.37±0.2	76.5±2.3	99.1±0.2
-400	25.0±2.1	0.8±0.3	74.2±2.3	99.9±0.1

Table S5. Faradaic efficiency of products for CO_2RR over Cu_7S_4/C-250 at different applied current densities.

Applied current density / mA cm^{-2}	FE H_2 / %	FE CO / %	FE C_2H_4 / %	FE CH_4 / %	FE $HCOO^-$ / %	FE Total / %
-100	39.5±3.2	0.2±0.2	-	-	59.2±2.7	98.9±0.8
-200	30.2±1.1	2.3±0.6	0.2±0.2	-	65.6±3.0	98.3±2.5
-300	31.6±2.7	0.9±0.3	0.1±0.1	-	67.5±3.4	100.0±0.5
-400	39.5±3.7	2.1±0.8	5.2±3.7	0.4±0.1	74.2±2.3	99.4±0.3

Table S6. Faradaic efficiency of products for CO_2RR over Cu_7S_4/C-350 at different applied current densities.

Applied current density / mA cm^{-2}	FE H_2 / %	FE CO / %	FE C_2H_4 / %	FE CH_4 / %	FE $HCOO^-$ / %	FE CH_3COO^- / %	FE C_2H_5OH / %	FE C_3H_7OH / %	FE Total / %
-100	30.3±2.7	12.5±4.9	5.8±0.9	-	33.9±3.1	1.2±0.8	14.9±4.1	1±1.4	99.6±0.3
-200	27.6±4.2	9.5±1.9	8.1±5.8	0.1±0.1	32.0±2.1	1.3±0.7	17.3±2.1	4.0±2.6	99.7±0.1
-300	23.7±1.1	5.9±2.2	17.0±5.9	1.5±1.1	30.0±5.4	2.2±1.5	18.2±2.9	1.3±1.9	99.9±0.2
-400	33.6±0.8	7.0±2.2	8.9±7.4	0.9±0.6	29.5±3.0	1.5±0.9	15.2±3.3	3.4±2.4	100.0±0.3

References：

1 W. Ma, S. Xie, X. G. Zhang, F. Sun, J. Kang, Z. Jiang, Q. Zhang, D. Y. Wu and Y. Wang, Nat. Commun., 2019, **10**, 892.

2 L. P. Chi, Z. Z. Niu, X. L. Zhang, P. P. Yang, J. Liao, F. Y. Gao, Z. Z. Wu, K. B. Tang and M. R.Gao, Nat. Commun., 2021, **12**, 5835.

3 X. Zheng, P. De Luna, F. P. García de Arquer, B. Zhang, N. Becknell, M. B. Ross, Y. Li, M. N. Banis, Y. Li, M. Liu, O. Voznyy, C. T. Dinh, T. Zhuang, P. Stadler, Y. Cui, X. Du, P. Yang and E. H. Sargent, Joule, 2017, **1**, 794—805.

4 W. He, I. Liberman, I. Rozenberg, R. Ifraemov and I. Hod, Angew. Chem. Int. Ed., 2020, **59**, 8262—8269.

5 T. Shinagawa, G. O. Larrazábal, A. J. Martín, F. Krumeich and J. Pérez-Ramírez, ACS Catal., 2018, **8**, 837—844.

6 Y. Deng, Y. Huang, D. Ren, A. D. Handoko, Z. W. Seh, P. Hirunsit and B. S. Yeo, ACS Appl. Mater. Interfaces, 2018, **10**, 28572—28581.

7 Y. Huang, Y. Deng, A. D. Handoko, G. K. L. Goh and B. S. Yeo, ChemSusChem 2018, 11, 320-326.

8 A. Zhang, Y. Liang, H. Li, S. Wang, Q. Chang, K. Peng, Z. Geng and J. Zeng, Nano Lett., 2021, **21**, 7789—7795.

9 Z. Tao, Z. Wu, Y. Wu and H. Wang, ACS Catal., 2020, **10**, 9271—9275.

10 T. Zheng, C. Liu, C. Guo, M. Zhang, X. Li, Q. Jiang, W. Xue, H. Li, A. Li, C. W. Pao, J. Xiao, C. Xia, J. Zeng, Nat. Nanotechnol., 2021, 16, 1386–1393.

11 L. X. Liu, X. Li, Y. Cai, H. Du, F. Liu, J. R. Zhang, J. Fu and W. Zhu, Nanoscale, 2022, **14**, 136793—13688.

12 K. Li, J. Xu, T. Zheng, Y. Yuan, S. Liu, C. Shen, T. Jiang, J. Sun, Z. Liu, Y. Xu, M. Chuai, C. Xia, and W. Chen, ACS Catal., 2022, **12**, 9922−9932.

13 Y. Shi, Y. Wang, J. Yu, Y. Chen, C. Fang, D. Jiang, Q. Zhang, L. Gu, X. Yu, X. Li, H. Liu, and W. Zhou, Adv. Energy Mater., 2023, 2203506

14 M. Tian, Sh. Wu, Y. Hu, Z. Mu, Z. Li, Y. Hou, P. Xi and C. H. Yana, Nanoscale, 2023, 15, 4477–4487

15 Y. Jiang, J. Shan, P. Wang, L. Huang, Y. Zheng and S. Z. Qiao, ACS Catal., 2023, **13**, 3101−3108